Coagulation-induced particle-concentration fluctuations in homogeneous, isotropic turbulence

Donald L. Koch
School of Chemical Engineering, Cornell University, Ithaca, New York 14853

Stephen B. Pope
Sibley School of Mechanical and Aerospace Engineering, Cornell University, Ithaca, New York 14853

(Received 24 September 2001; accepted 26 March 2002; published 5 June 2002)

The turbulent coagulation of micron-sized colloidal particles in a liquid is controlled by the shearing motion produced by Kolmogorov scale eddies. The rate of energy dissipation has fluctuations which vary over the integral length and time scale in a homogeneous, isotropic turbulent flow. We present a model of the particle concentrations and coagulation rates in a set of fluid packets that are large compared with the Kolmogorov scale and small compared with the integral scale. Particle coagulation occurs rapidly in regions of the flow with large dissipation rates, leading to a depletion of singlet particles. Thus, the singlet number density is negatively correlated with the shear rate. Turbulent mixing mitigates these concentration variations and the particle concentration field becomes nearly uncorrelated with dissipation rate in very dilute suspensions with $\phi R_\lambda \ll 1$. Here, ϕ is the particle volume fraction and R_λ is the Reynolds number based on the Taylor microscale. A simulation of a suspension of coalescing drops shows that the imperfect mixing at finite ϕR_λ broadens the drop size distribution. © *2002 American Institute of Physics.*
[DOI: 10.1063/1.1478562]

I. INTRODUCTION

Previous theoretical studies[1,2] of coagulation in homogeneous, isotropic turbulent flows have assumed a very dilute suspension which is well mixed on length scales larger than the particle diameter. Investigators performing direct-numerical simulations (DNS) of the coagulation rate in hydrosol and aerosol systems[3,4] have endeavored to use a sufficiently small particle volume fraction so that the particle concentration does not influence the interparticle collision rate. The rate at which single particles combine to form doublets due to coagulation is proportional to the square of the number density n of singlets and grows with increasing turbulent shear rate $\Gamma = \sqrt{\epsilon/\nu}$ or the instantaneous rate of energy dissipation ϵ. Here, ν is the kinematic viscosity of the fluid. The energy dissipation, which is controlled by the rate at which energy is extracted from the large scale turbulent motions, has large fluctuations and varies over the integral length and time scales. Singlet particles are preferentially depleted in regions of the flow characterized by large turbulent shear rates Γ, leading to a negative correlation between n and Γ. In a very dilute suspension, turbulent mixing will minimize the coagulation-induced particle concentration fluctuations. However, at higher concentrations, the negative correlations between the fluctuations in n and Γ over distances comparable with the integral length scale lead to a decrease in the overall rate of coagulation. In this paper, a stochastic model is presented that characterizes the magnitude of the coagulation-induced particle concentration fluctuations in an isotropic, homogeneous turbulent flow. This model is used to assess the effect of these fluctuations on the overall coagulation rate and particle size distribution and to determine when the dilute theories of particle coagulation[1,2] are appropriate.

Turbulent shearing motion is typically the dominant mechanism driving the coagulation of particles with radii a of about 0.5–5 μm.[5] The coagulation of smaller particles is controlled by Brownian motion. The coagulation of larger particles is dominated by differential sedimentation or turbulent accelerations, provided that there is some difference of size or density of the particles. The shearing motion in a turbulent flow is dominated by the smallest eddies whose size is characterized by the Kolmogorov length scale $l_K = (\nu^3/\langle\epsilon\rangle)^{1/4}$, where $\langle\ \rangle$ indicates an ensemble average. The shear rate produced by these eddies is $\Gamma = (\epsilon/\nu)^{1/2}$. In most laboratory, industrial, and environmental flows, the Kolmogorov length lies in the range of 50 μm–1 mm. It is therefore much larger than the size of the aggregating particles and this observation implies that it is only the local linear flow characterized by Γ that influences the aggregation process. Because the Reynolds number based on the Kolmogorov scale variables $\langle\Gamma^2\rangle^{1/2} l_K^2/\nu$ is defined to be 1, the particle Reynolds number $R_p = \langle\Gamma^2\rangle^{1/2} a^2/\nu$ is much less than one and fluid inertia may be neglected during particle–particle encounters. For particles suspended in liquids, the mass densities of the particle and fluid are comparable and the particle inertia is also negligible, i.e., the Stokes number $\mathrm{St} = (2/9)\rho_p \langle\Gamma^2\rangle^{1/2} a^2/\mu \ll 1$. Here, ρ_p is the density of the dispersed phase and μ is the dynamic viscosity of the continuous phase. In this paper, we will restrict our attention to the case of negligible particle inertia.

The rate r^* of coagulation, defined as the number of

coagulation events per unit volume per unit time in which two particles of radius a combine to form a doublet, is given by

$$r^* = -\frac{dn}{dt} = kn^2, \tag{1}$$

where k is the rate constant. If we neglect hydrodynamic and colloidal interactions among the particles as well as particle inertia, then the only dimensional quantities that k can depend on are the turbulent shear rate Γ and the particle radius a. Thus,

$$k = \alpha \Gamma a^3, \tag{2}$$

where α is a dimensionless constant. Saffman and Turner[1] considered the local linear flow in the vicinity of a colliding particle pair to be a purely extensional flow, characterized by a velocity gradient tensor that did not change during the $O(\Gamma^{-1})$ time required for an interparticle encounter. This led to a prediction that $\alpha = 10.35$. Brunk *et al.*[2] simulated the relative motion of particle pairs in a linear flow field with a velocity gradient that varied stochastically with time. The moments of the velocity gradient field were isotropic and the autocorrelation of each component of the strain rate and of the vorticity reproduced the values obtained for Lagrangian particles in direct-numerical simulations of isotropic turbulence.[6] These simulations taking account of the temporal variations of the velocity gradient yielded $\alpha = 8.62$.[7]

Brunk *et al.* also performed simulations that included the hydrodynamic interactions and van der Waals attractions between the particles. In a continuum fluid, hydrodynamic interactions provide a viscous resistivity that diverges at small separations and would prevent any coalescence from occurring in the absence of van der Waals attractions. The simple case, in which only van der Waals and hydrodynamic forces act, can be realized in a suspension in which the electrolyte concentration is sufficiently high to screen the electrostatic interactions at any appreciable interparticle separation. The coefficient α in this case depends on $N_s = 12\pi\mu a^3\Gamma/A$, the ratio of viscous to van der Waals forces and $N_L = 4\pi a/\lambda$. Here, A is the Hamaker constant and λ is the retardation length for the van der Waals attractions. For sufficiently large particles and high shear rates, i.e., $N_s > 10$ and $N_s > (N_L/500)^2$, the simulation results could be fit with a simple power law

$$\alpha = 0.52 N_s^{-0.16}. \tag{3}$$

Typically, the net effect of particle interactions is to decrease the coagulation rate by a factor of order 10 and to slightly decrease the sensitivity of the coagulation to the shear rate.

The theories of Saffman and Turner[1] and Brunk *et al.*[2] assume that the suspension is well mixed, so that the probability of finding two particles separated by any distance large compared with $2a$ is equal to the square of a number of particles per unit volume, which does not fluctuate with position. In this paper, we will extend these results to account for the number density fluctuations that occur in a nondilute coagulating hydrosol.

II. STOCHASTIC MODEL

The theories of Saffman and Turner[1] and Brunk *et al.*[2] describe the coagulation of hydrosols occurring on length and time scales comparable with the Kolmogorov scale. The dissipation rate in a turbulent flow will vary over the much larger integral time and length scales and, in a nondilute suspension, these variations will result in large-scale variations in the particle number density. In the presence of these large-scale inhomogeneities, Eq. (2) still provides the correct relationship of the local rate of coagulation to the local dissipation rate and particle number density.

To model the shear-rate and number-density variations, we will consider the flow to consist of a set of many suspension packets. The packet size is much larger than the Kolmogorov length scale and is large enough to contain many particles, but it is much smaller than the integral length scale. Thus, each fluid packet has a dissipation rate ϵ and equivalent Kolmogorov shear rate Γ and number density of singlets n. Because the packet size is small compared with the integral length scale, these quantities can be assumed to be uniform within each packet. To illustrate the effects of mixing on the coagulation process, we will first consider a simple model in which two particles are removed from the simulation rather than forming a larger particle when they collide. This model has been used in direct-numerical simulations of turbulent coagulation[3] and it is qualitatively consistent with the actual situation in which the total rate of collision of singlets with particles of all sizes decreases as the mean size of the neighboring particles grows. In the final section, we will treat a more realistic model in which drops coalesce on contact to form larger drops. The time variation of the number density in each packet is given by

$$\frac{dn}{dt} = -\alpha\Gamma n^2 a^3 - \left[\frac{n - \langle n\rangle}{\tau_m}\right] + S, \tag{4}$$

where the first term on the right-hand side is the loss of singlets due to coagulation, the second term is a model for turbulent mixing of particles between the packets, and the third term S is a source of particles per unit volume. For the majority of the calculations we will consider noninteracting particles so that $\alpha = 8.62$. The source, which is a constant, is added in some of the calculations so as to produce a statistical steady state for n. The mixing term in (4) is the "interaction by exchange with the mean" mixing model,[8] in which $\langle n\rangle$ is the mean number density (i.e., the average over all packets). This model is commonly used for single-phase mixing in probability distribution function modeling of turbulent flows;[9] and we use here the standard value of the mixing rate.

$$\frac{1}{\tau_m} = \frac{C_\phi\langle\epsilon\rangle}{2k} = \frac{1}{T_E}, \tag{5}$$

where the Eulerian integral time scale T_E is defined as the ratio of the turbulent kinetic energy k to the mean dissipation rate $\langle\epsilon\rangle$, and the model constant C_ϕ takes the value 2.0. Note that $\langle\Gamma^2\rangle^{1/2} T_E = (\frac{3}{20})^{1/2} R_\lambda$, where $R_\lambda = u'\lambda/\nu$ is the Reynolds number based on the turbulent velocity $u' = (2k/3)^{1/2}$ and the Taylor microscale, λ, which is related to the rate of

energy dissipation by $\lambda=(15\nu u'^2/\langle\epsilon\rangle)^{1/2}$. The use of a mixing model developed for mixing of passive scalar quantities in a single-phase flow for the mixing of particles or droplets can be justified because: (a) the particles are assumed to be sufficiently dilute that they do not affect the flow; and (b) they are small and have negligible inertia so that they follow the large-scale motion of the fluid.

The variations in the Kolmogorov shear rate are modeled in a manner similar to that proposed by Girimaji and Pope.[10] Pope[11] noted that the logarithm of the Kolmogorov shear rate can be divided into two parts

$$\Gamma=\langle\Gamma\rangle\exp[\chi+\psi], \tag{6}$$

where ψ varies over the Kolmogorov time scale and χ over the integral time scale. The stochastic variables ψ and χ are modeled to vary according to the Ornstein–Uhlenbeck processes

$$d\chi=-\left(\chi+\frac{1}{2}\sigma_\chi^2\right)\frac{dt}{\tau_\chi}+\left(\frac{2\sigma_\chi^2}{\tau_\chi}\right)^{1/2}dW_\chi \tag{7}$$

and

$$d\psi=-\left(\psi+\frac{1}{2}\sigma_\psi^2\right)\frac{dt}{\tau_\psi}+\left(\frac{2\sigma_\psi^2}{\tau_\psi}\right)^{1/2}dW_\psi, \tag{8}$$

where dW_χ and dW_ψ are independent Wiener processes, i.e., $\langle dW_i\rangle=0$ and $\langle dW_i^2\rangle=dt$ for $i=\chi$ and ψ. This model captures the log-normal distributions of the Kolmogorov shear rate Γ and dissipation rate ϵ. It also reproduces approximately the autocorrelation function of $\ln(\epsilon)$ observed in DNS. In particular, it yields an exponential temporal decay of the autocorrelation function at short times with a time scale that is proportional to the Kolmogorov time scale and a second region of exponential decay at long times with a time constant that scales with the integral time. The variances, σ_χ^2 and σ_ψ^2, and the ratios of the time scales to the integral time, τ_χ/T_E and τ_ψ/T_E, are derived from previous theoretical, DNS, and experimental results in the Appendix.

Typically, calculations were performed using 10 000 suspension packets to obtain good statistics. Equation (4) for the number density was solved by forward Euler integration. The linearity of (7) and (8) was exploited to provide a time update that exactly reproduces the probability distributions for $\chi(t+dt)$ and $\psi(t+dt)$ conditioned on the values of χ and ψ at time t.

III. RESULTS FOR COAGULATION-INDUCED CONCENTRATION FLUCTUATIONS AND COAGULATION RATE

In this section, we present results of the stochastic simulations for the turbulence-induced particle concentration fluctuations using the simple model in which the collision of particles results in their annihilation. In most of the calculations, we introduce a constant source of particles throughout the suspension to balance those that are removed by collision events. This eventually leads to a statistical steady state for the particle volume fractions $\phi=n(4\pi a^3/3)$ and Kolmogorov shear rates of the suspension packets. Figure 1 gives a scatter plot of the volume fractions and shear rates of the packets for $R_\lambda=500$ and an average volume fraction of $\langle\phi\rangle=0.001\,08$. It can be seen that there is a strong negative correlation between the particle concentration and the shear rate. This results from the higher coagulation rates experienced by particles in the high-shear-rate regions. This negative correlation between ϕ and Γ leads to a decrease in the coagulation rate compared with that which would occur in a well-mixed suspension. The ratio of the coagulation rate to that in a well-mixed system is given by $r=\langle\Gamma\phi^2\rangle/\langle\Gamma\rangle\langle\phi\rangle^2$ and $r=0.860$ for the example shown in Fig. 1.

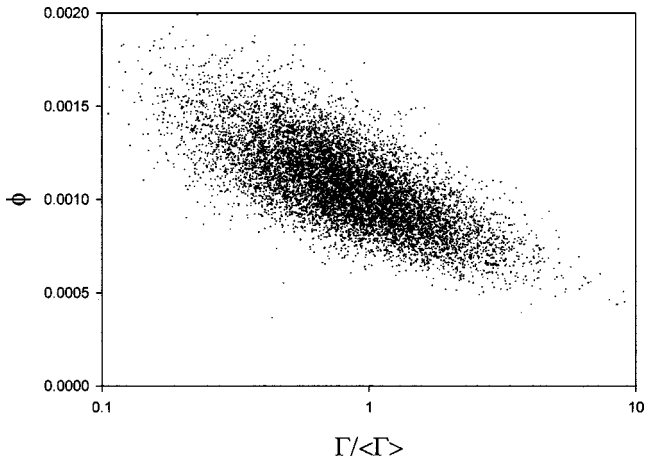

FIG. 1. The values of particle volume fraction and Kolmogorov shear rate are plotted for 10 000 fluid packets in a suspension with $R_\lambda=500$ and $\langle\phi\rangle=0.001\,08$. For these conditions the ratio of the coagulation rate to that occurring in the absence of mixing limitations is $r=0.860$, the particle velocity variance is $\langle\phi'^2\rangle/\langle\phi\rangle^2=0.043$, and the correlation between particle concentration and shear rate is $\langle\Gamma'\phi'\rangle/(\langle\Gamma\rangle\langle\phi\rangle)=-0.094$.

The ratio of the rate of coagulation to that in a well-mixed system is plotted as a function of particle volume fraction for several values of R_λ in Fig. 2. The well-mixed result is recovered at sufficiently small particle volume fractions, but the rate decreases with increasing ϕ. The rate of decrease in the coagulation rate with particle volume fraction

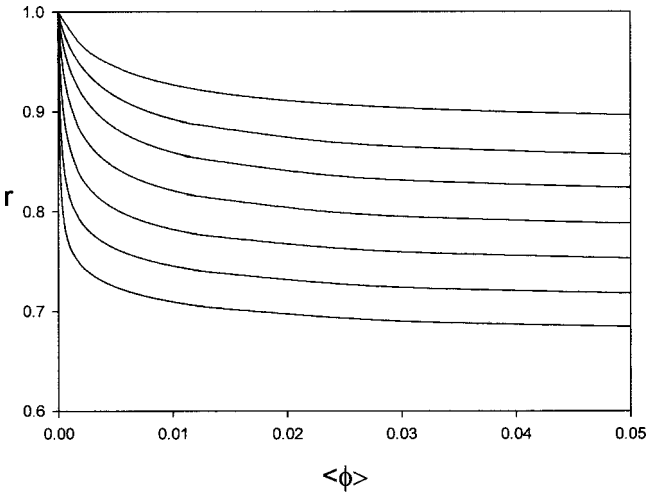

FIG. 2. The ratio of the coagulation rate to that in the absence of mixing limitations is plotted as a function of the average volume fraction for R_λ = 24, 62.5, 125, 250, 500, 1000, and 2000. The Reynolds number increases monotonically from the top curve to the bottom curve.

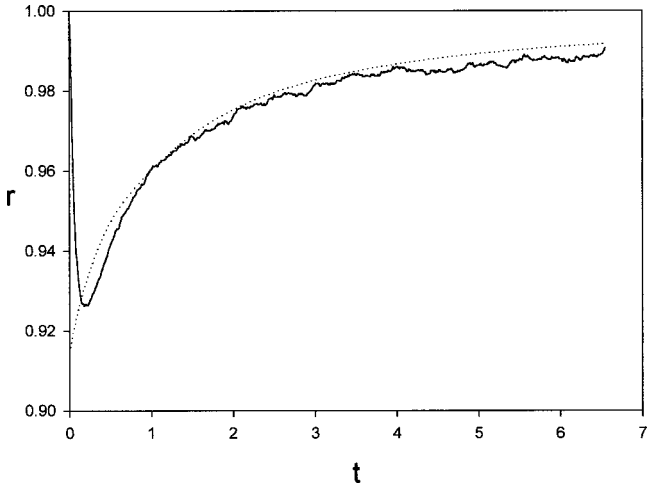

FIG. 3. The coagulation-rate ratio r is plotted as a function of time nondimensionalized by the Eulerian integral time T_E for $R_\lambda = 24$. The initial particle volume fraction is 0.0168 and the suspension is initially well mixed. The solid line is the simulation result. The dashed line is a quasisteady approximation obtained using the results from Fig. 2 for a stochastic steady state with the same mean volume fraction as that obtained at time t in the transient calculation.

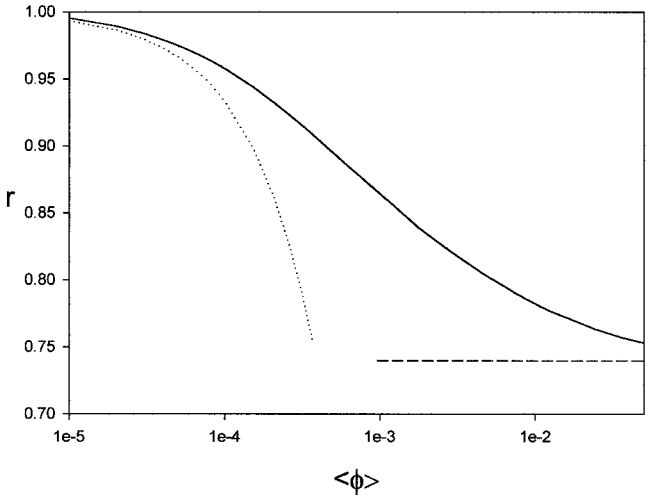

FIG. 4. The coagulation-rate ratio is plotted as a function of average volume fraction for $R_\lambda = 500$. The dotted and dashed lines indicate the small and large $\langle\phi\rangle R_\lambda$ asymptotes, respectively.

increases with increasing R_λ. This may be understood if we note that the coagulation process changes ϕ in a time of order $1/(\Gamma\langle\phi\rangle)$ while the turbulent mixing of particles among fluid packets and variations in the dissipation rate within each packet occur over the integral time scale T_E. Thus, the well-mixed condition holds only if $T_E \ll 1/(\Gamma\langle\phi\rangle)$ or $R_\lambda\langle\phi\rangle \ll 1$. At sufficiently high $R_\lambda\langle\phi\rangle$, the turbulent mixing is very slow compared with coagulation and r reaches a plateau that is determined by the variation of Γ within the flow. This plateau becomes lower at higher R_λ where the fluctuations in Γ are larger. These results indicate that mixing limitations are likely to be more prevalent at the higher Reynolds numbers that are often characteristic of geophysical applications than at the lower Reynolds numbers probed by DNS studies and many laboratory experiments.

The results in Figs. 1 and 2 were obtained using a source of particles to achieve a statistical steady state distribution of particle concentration among the fluid packets. To demonstrate that this method of analysis produces a quasisteady state approximation, we compare it with the results of a transient calculation. Wang *et al.*[3] introduced an initially uniform array of particles with volume fraction $\phi_0 = 0.0168$ into a DNS of isotropic turbulence with $R_\lambda = 24$ and observed the subsequent coagulation process. Scheme 3 in their paper corresponds to the assumption of particle annihilation on collision adopted in this section. We performed a corresponding simulation by setting the initial number density in each fluid packet to 0.0168 and omitting the source S. The rate r is plotted as a function of time nondimensionalized by T_E in Fig. 3. The solid line is the rate computed from the transient calculation. Because the system is initially well mixed, the initial rate is $r = 1$. As the coagulation proceeds, particles are depleted preferentially from high shear rate regions, so that r decreases. With time, however, the volume fraction of particles throughout the system decreases. This slows the coagulation process and allows time for turbulent mixing to reestablish a more homogeneous particle distribution. The dashed line is the quasisteady approximation obtained by applying the steady state results from Fig. 2 at the mean volume fraction obtained in the simulation at time t. It is seen that, after an initial adjustment period, the quasisteady state approximation accurately predicts the transient results. The initial volume fraction in Wang *et al.* was intended to be sufficiently small so that mixing limitations would not affect the coagulation rate. Our calculations confirm that the deviation from the well-mixed condition would be small, i.e., less than 8%. It should be noted, however, that the requirement to achieve good mixing would become more stringent as the Reynolds number of the simulations was increased. Wang *et al.* noted that their particles developed a bias toward regions of low energy dissipation and quantified this effect by plotting the ratio of the mean dissipation rate experienced by the particles to the mean dissipation rate in the fluid in their Fig. 8(b). Our results for this quantity, i.e., $\epsilon_p/\langle\epsilon\rangle = \langle\Gamma^2\phi\rangle/\langle\Gamma^2\rangle\langle\phi\rangle$, exhibit a similar trend to those for r. They decrease from 1, pass through a minimum of 0.990, and then grow to approach 1 again as $t \to \infty$. The results from the DNS of Wang *et al.* start from the well-mixed state $\epsilon_p/\langle\epsilon\rangle = 1$ at $t = 0$. The dissipation rate seen by the particles then decreases and fluctuates about a mean value of about 0.99. The DNS results do not show evidence of the recovery to the well-mixed state predicted by the stochastic model, but the statistical uncertainty in the DNS results is substantial and grows with time as the particles are depleted from the simulation domain.

Figure 4 shows the stochastic simulation results (solid line) for the rate ratio r as a function of mean particle volume fraction for $R_\lambda = 500$ using the model for high R_λ along with the asymptotic results for high and low $R_\lambda\langle\phi\rangle$. At sufficiently large values of $R_\lambda\langle\phi\rangle$, the coagulation occurs much more rapidly than turbulent mixing and temporal variations in the dissipation rate in a Lagrangian reference frame. In this case, the particle concentration in each fluid packet ad-

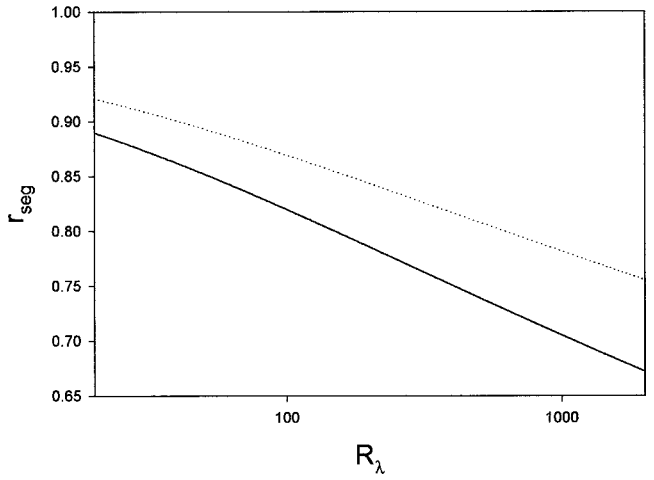

FIG. 5. The coagulation rate ratio in the limit of large $\langle\phi\rangle R_\lambda$ is plotted as a function of R_λ. The solid line indicates the result in the absence of particle interactions and the dotted line results based on the collision efficiency (3) that includes van der Waals attractions and hydrodynamic interactions.

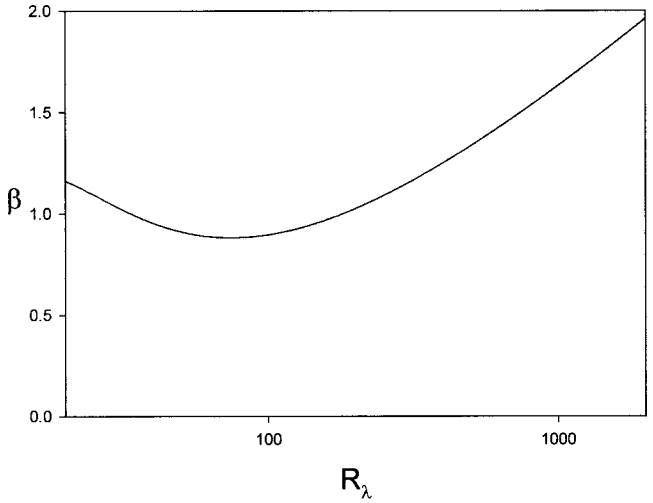

FIG. 6. The coefficient β in the expression (15) for the coagulation rate ratio at small $\langle\phi\rangle R_\lambda$ is plotted as a function of R_λ.

justs to a quasisteady balance of the source S and the coagulation rate $\alpha\Gamma n^2$, so that $n=(S/(\alpha\Gamma))^{1/2}$. Using this result, we can determine the mean number density for a given S and thereby the coagulation rate r_{seg} for a fully segregated state

$$r_{\text{seq}}=\exp(-\tfrac{3}{4}[\sigma_\chi^2+\sigma_\psi^2]). \tag{9}$$

This large $R_\lambda\langle\phi\rangle$ asymptote is plotted as the dashed line in Fig. 4. The variation of r_{seg} with Reynolds number is illustrated in Fig. 5. The segregation coagulation rate decreases nearly linearly with $\ln(R_\lambda)$ due to the growth of the variance of $\ln(\Gamma)$ with Reynolds number.

In the presence of colloidal interactions, the coagulation rate has a nonlinear dependence on the shear rate. For sufficiently large shear rates and particle diameters, the coagulation rate is proportional to $\Gamma^{0.84}\phi^2$, cf. (3). Thus, the coagulation rate is a weaker function of shear rate in the presence of colloidal interactions. As a result, the depletion of particle concentration in high shear regions is not as striking and the reduction of the coagulation rate is not as great. In the presence of particle interactions,

$$r_{\text{seq}}=\exp\left(-\frac{1323}{2500}[\sigma_\chi^2+\sigma_\psi^2]\right). \tag{10}$$

The result for r_{seg} (dashed line) in the presence of particle interactions can be compared to the result (solid line) without particle interactions in Fig. 5.

A theory valid for small $\langle\phi\rangle R_\lambda$ can be derived by realizing that, in this limit, the system is almost perfectly mixed and the fluctuations in particle volume fraction are very weak, i.e., $\phi'\ll\langle\phi\rangle$. For a nearly constant particle volume fraction, the coagulation rate and source terms in (4) may be simplified to yield

$$\frac{d\phi'}{dt}+\frac{\phi'}{\tau_m}=-\tilde{\alpha}\Gamma'\langle\phi\rangle^2, \tag{11}$$

where $\tilde{\alpha}=36.1$ in the absence of particle interactions. Integrating (11), to relate ϕ' to the previous history of the shear rate fluctuations, we can express the shear rate volume fraction correlation in terms of the shear rate autocorrelation, i.e.,

$$\langle\Gamma'\phi'\rangle=-\tilde{\alpha}\langle\phi^2\rangle\int_0^\infty\exp\left(-\frac{\tau}{\tau_m}\right)\langle\Gamma'(\tau)\Gamma'(0)\rangle d\tau. \tag{12}$$

Using the fact that $\chi(\tau)$ and $\chi(0)$ are modeled as joint normal variables, the shear rate correlations are found to be

$$\frac{\langle\Gamma'(\tau)\Gamma'(0)\rangle}{\langle\Gamma\rangle^2}=[\exp(\sigma_\chi^2)-1]\exp(-|\tau|/\tau_\chi)+[\exp(\sigma_\psi^2)-1]\exp(-|\tau|/\tau_\psi). \tag{13}$$

Substituting (13) into (12) yields

$$\langle\Gamma'\phi'\rangle=-\tilde{\alpha}\langle\phi\rangle^2\langle\Gamma\rangle^2\left\{\frac{\tau_m\tau_\chi}{\tau_m+\tau_\chi}[\exp(\sigma_\chi^2)-1]+\frac{\tau_m\tau_\psi}{\tau_m+\tau_\psi}[\exp(\sigma_\psi^2)-1]\right\}. \tag{14}$$

At sufficiently small volume fractions, then, the rate of coagulation may be approximated as

$$r=1+\frac{\langle\Gamma'\phi'\rangle}{\langle\Gamma\rangle\langle\phi\rangle}=1-\beta R_\lambda\langle\phi\rangle, \tag{15}$$

where β is plotted as a function of R_λ in Fig. 6. The linear dependence of the decay of the coagulation rate written explicitly in (15) reflects the influence of the difference in time scales between the coagulation process on one hand and the mixing process and the variations in dissipation rate on the other. The additional Reynolds number dependence shown in the plot of β in Fig. 6 arises from the decrease in τ_χ/T_{E} and τ_ψ/T_{E} at small and moderate R_λ and from the growth of the variance of the dissipation rate with R_λ, cf. Figs. 13 and 11.

The variance of the particle volume fraction at small $\langle\phi\rangle R_\lambda$ can be derived in a similar manner and one obtains

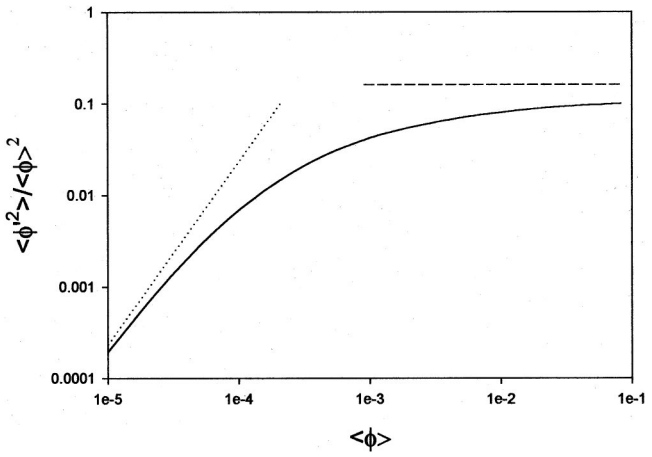

FIG. 7. The variance of the particle volume fraction is plotted as a function of mean volume fraction for $R_\lambda = 500$. The solid line represents the simulation results, the dotted line is the small $\langle\phi\rangle R_\lambda$ asymptote $\langle\phi'^2\rangle = 5.2 \times 10^4 \langle\phi\rangle^4$, and the dashed line is the large $\langle\phi\rangle R_\lambda$ asymptote $\langle\phi'^2\rangle = 0.162\langle\phi\rangle^2$.

$$\langle\phi'^2\rangle = \tilde{\alpha}^2\langle\phi\rangle^4\langle\Gamma\rangle^2\left\{\frac{\tau_m^2\tau_\chi}{\tau_m+\tau_\chi}[\exp(\sigma_\chi^2)-1] + \frac{\tau_m^2\tau_\psi}{\tau_m+\tau_\psi}[\exp(\sigma_\psi^2)-1]\right\}. \tag{16}$$

This indicates that the particle volume fraction variance is proportional to $\langle\phi\rangle^4 R_\lambda^2$ in the dilute limit. Figure 7 shows the particle volume fraction variance obtained from the stochastic simulations for $R_\lambda = 500$ (solid line) compared with this dilute asymptote (dotted line). The normalized volume fraction variance grows rapidly with particle concentration at small concentrations but approaches a constant

$$\frac{\langle\phi'^2\rangle}{\langle\phi\rangle^2} = \exp\left[\frac{3}{4}(\sigma_\chi^2+\sigma_\psi^2)\right]-1 \tag{17}$$

predicted by the segregation model at high concentrations. For $R_\lambda = 500$, the variance predicted by the segregation model for $\phi R_\lambda \gg 1$ is $\langle\phi'^2\rangle = 0.162\langle\phi\rangle^2$, which is indicated by the dashed line in Fig. 7.

IV. DROP SIZE DISTRIBUTION

We will now briefly consider the evolution of the size distribution in a suspension of drops coalescing due to turbulence-driven collisions. It will be assumed that collision of two drops leads to the formation of a larger drop with a volume equal to the sum of the volumes of the colliding drops. In addition, drop break up due to the turbulent flow will be neglected. These assumptions are reasonable for small drops, which have a small Capillary number $\mathrm{Ca} = \mu\Gamma a/\sigma$ and do not deform appreciably due to the flow. Here, σ is the surface tension of the drop interface. A system of coalescing drops is simpler than one consisting of particle aggregates, because the larger drops formed due to coalescence events are spherical. For such a polydisperse suspension, the rate expression (1) can be replaced by the rate of collision of drops of species i and j, i.e.,

$$r_{ij}^* = k_{ij} n_i n_j, \tag{18}$$

where the rate coefficient k_{ij} is given by

$$k_{ij} = 8.62\Gamma\left(\frac{a_i+a_j}{2}\right)^3 \tag{19}$$

and a_i is the radius of the ith species. As in Sec. III, we consider the fluid to consist of a set of fluid packets each with its own Kolmogorov shear rate. In the present case, however, each packet contains a set of drops with different radii. We consider an initially monodisperse suspension of drops with radius a_1. The coalescence of these drops leads to a discrete set of drop sizes

$$a_i = i^{1/3} a_1. \tag{20}$$

To achieve a steady state size distribution, we will consider a model in which each fluid packet receives an inlet stream consisting of droplets of species 1 with a volume fraction ϕ_{10} equal to the initial volume fraction in the suspension. An outlet stream with an equal volumetric flow rate is extracted from each packet. This is similar to the common model of a continuous stirred-tank reactor. Thus, the number density of species i in each packet evolves according to

$$\frac{dn_i}{dt} = -\sum_{j=1}^{N} k_{ij} n_i n_j + \frac{1}{2}\sum_{j=1}^{i-1} k_{j,i-j} n_j n_{i-j} - \left(\frac{n_i - \langle n_i\rangle}{\tau_m}\right) - \left(\frac{n_i - \delta_{i1} n_{10}}{\tau_r}\right), \tag{21}$$

where N is the total number of drop sizes considered in the calculation and $n_{10} = \phi_{10}/(\frac{4}{3}\pi a_1^3)$. The residence time in the system, τ_r, is equal to the ratio of the system volume to the volumetric flow rate of the inlet stream.

We computed the drop size distribution for $R_\lambda = 2000$ for a range of particle volume fractions. Forty drop sizes were considered in the calculation. Any drop–drop collisions that should have resulted in the formation of larger drops than those considered in the calculations led to a loss of mass from the system. For the parameter regime explored this loss of mass was always less than 1.5% of the total mass of the drops in the system. The computations were performed with 100 fluid packets. The residence time was taken to be $\tau_r = 1/(R_\lambda \phi_{10})$. By scaling the residence time with $1/\phi_{10}$, we assured that the size distribution for a perfectly mixed system would be independent of ϕ_{10}.

In keeping with the results obtained for the simple annihilation model in Sec. III, we expect that the mixing limitations that arise at higher particle volume fractions will reduce the initial stages of the coagulation process and so reduce the mean radius of the droplets. On the other hand, the variations of the Kolmogorov shear rate in various parts of the fluid will cause some regions to develop quite large drops while little coalescence occurs in other regions. This will tend to broaden the size distribution. These effects can be observed in Fig. 8, which illustrates the size distribution for a well-mixed suspension (dashed line) with a very small volume fraction $R_\lambda\langle\phi\rangle = 1/4$ and the distribution for a higher volume fraction suspension $R_\lambda\langle\phi\rangle = 16$ (solid line). The mixing limi-

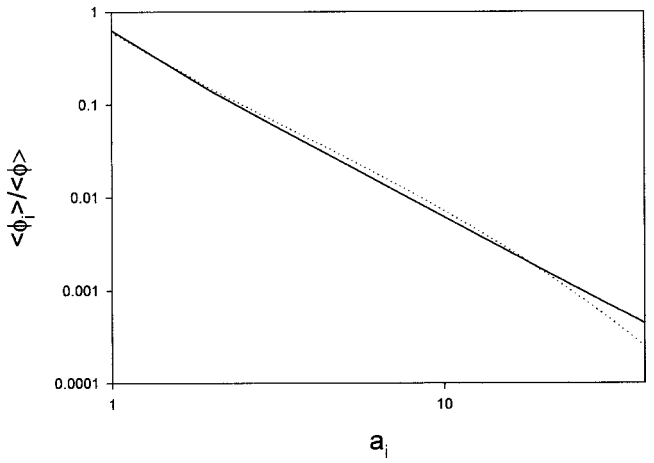

FIG. 8. The drop size distribution is plotted for $R_\lambda = 2000$ with $R_\lambda\langle\phi\rangle = 1/4$ (dashed line) and $R_\lambda\langle\phi\rangle = 16$. The ordinate is the fraction of the total drop volume consisting of drops with radius a_i.

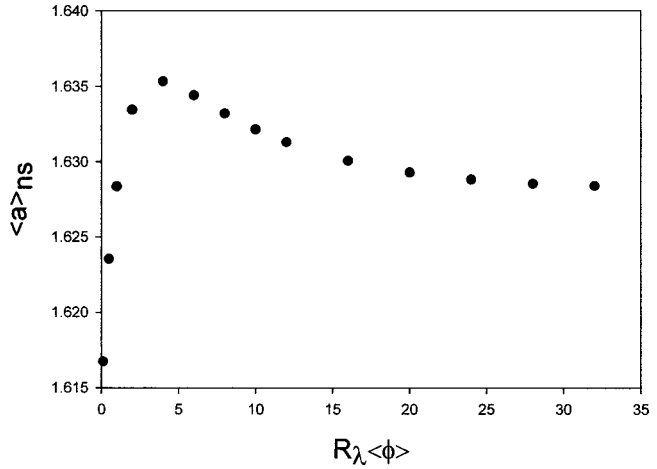

FIG. 10. The mean radius of the nonsinglet drops is plotted as a function of volume fraction for $R_\lambda = 2000$.

tations in the higher volume fraction suspension lead to a smaller volume fraction of doublets and triplets than in the dilute suspension, indicating that the initial coagulation rate is suppressed. However, the largest droplets are more evident in the poorly mixed suspension. Figure 9 is a plot of the mean droplet size as a function of volume fraction. The size decreases with increasing volume fraction and eventually approaches a large $R_\lambda\langle\phi\rangle$ asymptote. These results are quite similar to the behavior of the coagulation rate given in Fig. 2. A simple measure of the breadth of the size distribution is to consider the mean size of the drops that are larger than a_1. This mean size of nonsinglet drops is plotted as a function of the volume fraction in Fig. 10. While the overall mean drop size decreases with increasing volume fraction, the mean size of the nonsinglets increases at first with volume fraction, passes through a maximum, and levels off at a value larger than the well-mixed result. This demonstrates that mixing limitations broaden the size distribution of coalescing drops.

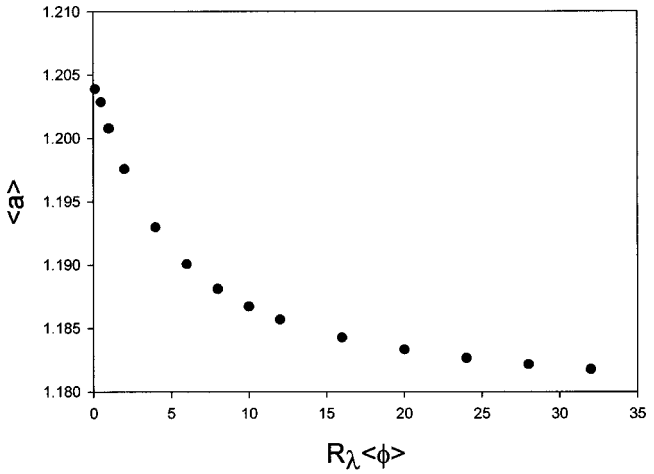

FIG. 9. The mean radius of drops in a turbulent flow with $R_\lambda = 2000$ is plotted as a function of the particle volume fraction.

V. CONCLUSIONS

We have examined the effects of the large scale variations in the turbulent dissipation rate in a homogeneous turbulent flow on turbulence-induced coalescence of drops or coagulation of particles. The variation in the Kolmogorov shear rate with position results in variations in the coagulation rate. As a result, the coagulation process induces fluctuations in the concentrations of singlet particles, doublets, etc. There is a negative correlation between the singlet particle concentration and the Kolmogorov shear rate, which reduces the overall rate of loss of singlets. We illustrated this effect using a simple model in which the collision of two singlets results in annihilation of the particles. The ratio of the coagulation rate to that in a well mixed system decreases with increasing volume fraction and with increasing Reynolds number and approaches an asymptote characteristic of a fully segregated state at large $R_\lambda\langle\phi\rangle$. The well mixed state is recovered only if $\langle\phi\rangle < 0.03/R_\lambda$, so that mixing limitations are more significant in higher Reynolds number flows. Finally, we briefly considered the size distribution of a suspension of droplets coalescing in a turbulent flow. Here, mixing limitations not only reduce the overall rate of coalescence as measured by the mean drop radius, but they also broaden the drop size distribution.

ACKNOWLEDGMENT

Financial support for this work was provided by NASA Grant No. NAG3-2349.

APPENDIX: STOCHASTIC MODEL FOR LAGRANGIAN TEMPORAL VARIATIONS OF THE KOLMOGOROV SHEAR RATE

The shear rate following a fluid particle $\Gamma(t)$ is modeled as

$$\ln[\Gamma(t)/\langle\Gamma\rangle] = \psi(t) + \chi(t), \tag{A1}$$

where $\psi(t)$ and $\chi(t)$ are independent Ornstein–Uhlenbeck (OU) processes. The two OU processes are defined by their variances σ_ψ^2 and σ_χ^2, and their time scales τ_ψ and τ_χ. (The

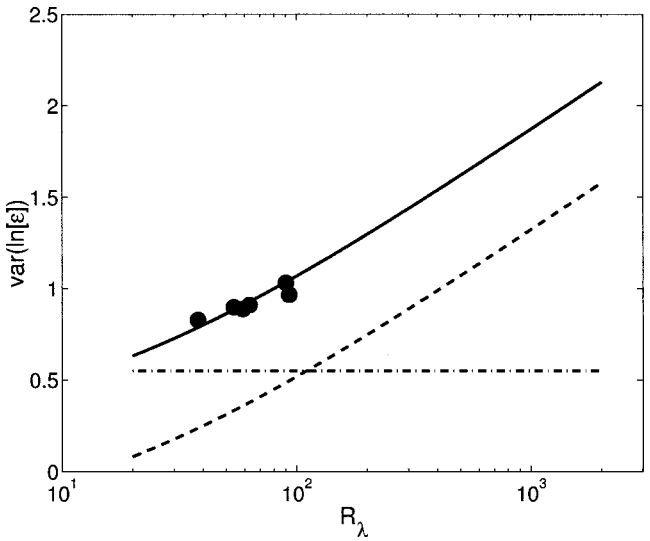

FIG. 11. Variance of $\ln \varepsilon$ against R_λ: solid line, var $(\ln \varepsilon)$, Eq. (A9); dot–dashed line $\sigma_\phi^2 = 0.55$; dashed line $\sigma_\theta^2 = \mathrm{var}(\ln(\varepsilon)) - \sigma_\phi^2$; symbols, DNS data of Yeung and Pope (Ref. 6).

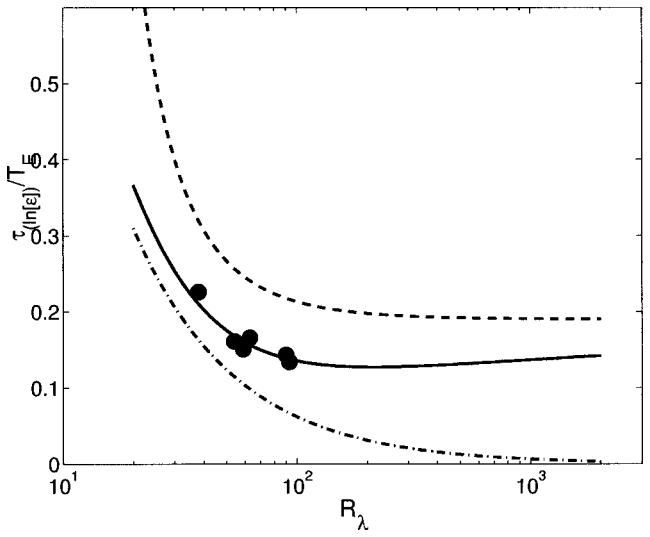

FIG. 13. Time scales of processes normalized by $T_E = k/\langle\varepsilon\rangle$: solid line, $\tau_{\ln\varepsilon}/T_E$, Eq. (A14); symbols, $\tau_{\ln\varepsilon}/T_E$, DNS of Yeung and Pope (Ref. 6); dashed line τ_θ/T_E, Eq. (A18); dot–dashed line, τ_ϕ/T_E, Eq. (A17).

means are specified as $-\frac{1}{2}\sigma_\psi^2$ and $-\frac{1}{2}\sigma_\chi^2$ for consistency with the normalization of Γ by its mean.) The purpose of this appendix is to provide appropriate specifications for the non-dimensional parameters σ_ψ^2, σ_χ^2, τ_ψ/T_E and τ_χ/T_E.

The current model for $\Gamma(t) = [\varepsilon(t)/\nu]^{1/2}$ is closely related to the model for $\varepsilon(t)$ proposed by Pope,[11] which can be written

$$\ln[\varepsilon(t)/\langle\varepsilon\rangle] = \phi(t) + \theta(t). \tag{A2}$$

The variances of the stationary random processes $\phi(t)$ and $\theta(t)$ are denoted by σ_ϕ^2 and σ_θ^2, and their integral time scales by τ_ϕ and τ_θ. [Note that in Ref. 11, $\theta(t)$ is denoted by $\psi(t)$, and that here τ_ϕ and τ_θ are defined as the integrals of the autocorrelation functions which differ from the definitions in Ref. 11.] From the relation $\Gamma = (\varepsilon/\nu)^{1/2}$ it follows that the parameters in the models for $\Gamma(t)$ and $\varepsilon(t)$ are related by

$$\tau_\psi = \tau_\phi, \quad \tau_\chi = \tau_\theta, \quad \sigma_\psi^2 = \tfrac{1}{4}\sigma_\phi^2, \quad \sigma_\chi^2 = \tfrac{1}{4}\sigma_\theta^2. \tag{A3}$$

Here we first provide a specification for the parameters in the model for $\varepsilon(t)$, and then use the above-mentioned equations to deduce the appropriate parameters in the model for $\Gamma(t)$.

As shown by Pope,[11] the autocorrelation functions of $\ln(\varepsilon/\langle\varepsilon\rangle)$ given by the model are in good agreement with those obtained from the DNS of Yeung and Pope[6] if the coefficients are specified by

$$\sigma_\phi^2 = 0.55, \quad \tau_\theta/\tau_\eta = 2.4, \quad \tau_\theta/T_L = 0.89, \tag{A4}$$

where τ_η is the Kolmogorov timescale, and T_L is the Lagrangian velocity integral time scale. The variance σ_θ^2 is obtained from the relation

$$\mathrm{var}(\ln \varepsilon) = \sigma_\phi^2 + \sigma_\theta^2, \tag{A5}$$

with the empirical expression for the variance of the logarithm of the dissipation

$$\mathrm{var}(\ln \varepsilon) = A + \mu \ln(L_{11}/\eta), \tag{A6}$$

where L_{11} is the longitudinal integral scale. The value of the intermittency exponent $\mu = 0.25$ is taken from Sreenivasan and Kailasnath;[12] and the constant $A = -0.15$ is chosen to match DNS data (as shown in the following, Fig. 11).

To complete the specification we need to relate the various scales that appear—τ_η, T_L, L_{11}/η—to R_λ and $T_E \equiv k/\langle\varepsilon\rangle$.

From the definition of the quantities involved we have $\tau_\eta/T_E = (20/3)^{1/2}/R_\lambda$, and hence from Eq. (A4)

$$\tau_\phi/T_E = 6.2/R_\lambda. \tag{A7}$$

With $L \equiv k^{3/2}/\langle\varepsilon\rangle$, the length scale ratio L_{11}/η is estimated as

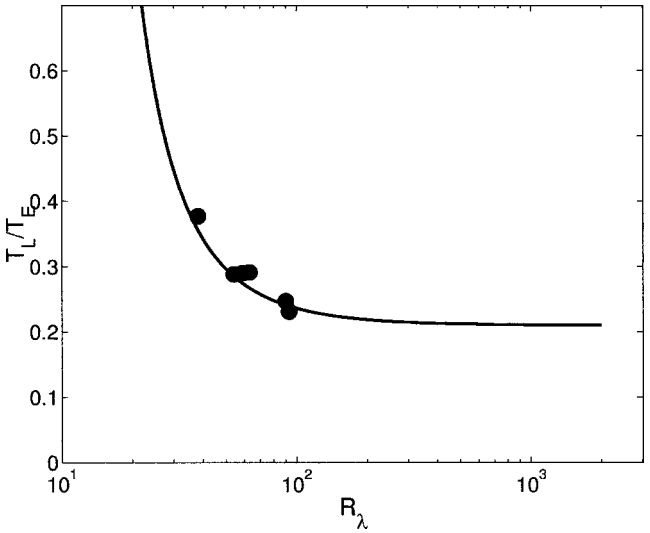

FIG. 12. Ratio of Lagrangian velocity integral time scale to $k/\langle\varepsilon\rangle$: line, Eq. (A13); symbols, DNS data of Yeung and Pope (Ref. 6).

$$L_{11}/\eta=(L_{11}/L)(L/\eta)=[0.43+12.8/R_\lambda]\left(\frac{3}{20}\right)^{3/4}R_\lambda^{3/2}, \quad \text{(A8)}$$

where the quantity in square brackets is a fit to the estimate of L_{11}/L given by Pope[9] (see Fig. 6.24). Thus Eqs. (A6) and (A8) yield

$$\mathrm{var}(\ln\varepsilon)=-0.15+0.25\ln(3.1R_\lambda^{1/2}+0.1R_\lambda^{3/2}). \quad \text{(A9)}$$

Figure 11 shows this estimate compared to the DNS data of Yeung and Pope.[6]

Finally, an estimate of T_L/T_E is obtained from Sawford's model for fluid particle acceleration,[13] as modified by Pope.[14] Equations (80), (83)–(86) of Pope[14] give

$$\frac{T_L}{T_E}=\frac{4}{3C_T}+\frac{\tau_\eta}{T_E}\frac{C_T}{2a_0}, \quad \text{(A10)}$$

where

$$C_T=6.2(1+4/R_\lambda), \quad \text{(A11)}$$

and a_0 is the Kolmogorov-scaled acceleration variance. From the DNS data of Vedula and Yeung,[15] we estimate

$$a_0=1.05\ln(0.1R_\lambda), \quad \text{(A12)}$$

which leads to

$$\frac{T_L}{T_E}=\frac{0.21}{1+4/R_\lambda}+\frac{7.6(1+4/R_\lambda)}{R_\lambda\ln(0.1R_\lambda)}. \quad \text{(A13)}$$

Figure 12 shows that this estimate agrees well with the DNS data; and that at $R_\lambda\approx 30$, T_L/T_E is about twice its high-Reynolds number asymptote.

As a check on these estimates, Fig. 13 shows the implied time scale of $\ln(\varepsilon)$,

$$\frac{\tau_{\ln\varepsilon}}{T_E}=\frac{\sigma_\phi^2\tau_\phi+\sigma_\theta^2\tau_\theta}{(\sigma_\phi^2+\sigma_\theta^2)T_E} \quad \text{(A14)}$$

compared to DNS data. Figure 13 also shows τ_ϕ/T_E and τ_θ/T_E.

In summary, the parameters specified in the model for $\Gamma(t)$ are

$$\sigma_\psi^2=\tfrac{1}{4}\sigma_\phi^2=0.14, \quad \text{(A15)}$$

$$\sigma_\chi^2=\tfrac{1}{4}\mathrm{var}(\ln\varepsilon)-\sigma_\psi^2=-0.18+\tfrac{1}{16}\ln(3.1R_\lambda^{1/2}+0.1R_\lambda^{3/2}), \quad \text{(A16)}$$

$$\frac{\tau_\psi}{T_E}=\frac{\tau_\phi}{T_E}=\frac{6.2}{R_\lambda}, \quad \text{(A17)}$$

$$\frac{\tau_\chi}{T_E}=\frac{\tau_\theta}{T_E}=\frac{0.19}{1+4/R_\lambda}+\frac{6.8(1+4/R_\lambda)}{R_\lambda\ln(0.1R_\lambda)}. \quad \text{(A18)}$$

[1] P.G. Saffman and J.S. Turner, "On the collision of drops in turbulent clouds," J. Fluid Mech. **1**, 16 (1956).

[2] B.K. Brunk, D.L. Koch, and L.W. Lion, "Turbulent coagulation of colloidal particles," J. Fluid Mech. **364**, 81 (1998).

[3] L.-P. Wang, A.S. Wexler, and Y. Zhou, "On the collision rate of small particles in isotropic turbulence. 1. Zero-inertia case," Phys. Fluids **10**, 266 (1998).

[4] S. Sundaram and L.R. Collins, "Collision statistics in an isotropic particle-laden turbulent suspension. 1. Direct numerical simulations," J. Fluid Mech. **335**, 75 (1997).

[5] H.R. Prupacher and J.D. Klett, *Microphysics of Clouds and Precipitation* (Reidel, Dordrecht, Netherlands, 1978).

[6] P.K. Yeung and S.B. Pope, "Lagrangian statistics from direct numerical simulations of isotropic turbulence," J. Fluid Mech. **207**, 531 (1989).

[7] Brunk *et al.* (Ref. 2) actually gave the rate of coagulation as twice the value specified here, because they took the number of particle pairs in the suspension to be n^2 instead of the appropriate expression $\frac{1}{2}n^2$ for indistinguishable particles.

[8] J. Villermaux and J.C. Devillon, in *Proceedings of the Second International Symposium on Chemical Reaction Engineering* (Elsevier, New York, 1972).

[9] S.B. Pope, *Turbulent Flows* (Cambridge University Press, Cambridge, 2000).

[10] S.S. Girimaji and S.B. Pope, "A stochastic model for velocity gradients in turbulence," Phys. Fluids A **2**, 242 (1990).

[11] S.B. Pope, "Lagrangian microscales in turbulence," Philos. Trans. R. Soc. London, Ser. A **333**, 309 (1990).

[12] K.R. Sreenivasan and P. Kailasnath, "An update on the intermittency exponent in turbulence," Phys. Fluids A **5**, 512 (1993).

[13] B.L. Sawford, "Reynolds number effects in Lagrangian stochastic models of turbulent dispersion," Phys. Fluids A **3**, 1577 (1991).

[14] S.B. Pope, "Lagrangian PDF methods for turbulent flows," Annu. Rev. Fluid Mech. **26**, 23 (1994).

[15] P. Vedula and P.K. Yeung, "Similarity scaling of acceleration and pressure statistics in numerical simulations of isotropic turbulence," Phys. Fluids **11**, 1208 (1999).